CONTENTS

1. PURPOSE OF PROCEDURE

2. EXAMPLE FOR RANS CFD CODE
     2.1 Geometry, Conditions, and Benchmark Data
     2.2 Grids
     2.3 Verification and Validation of Integral Variable: Resistance
     2.4 Verification and Validation of Point Variable: Wave Profile

3. REFERENCES

INTERIM RECOMMENDED PROCEDURE
PREPARED BY RESISTANCE COMMITTEE OF 22nd ITTC

Edited	Approved
Date	Date

Uncertainty Analysis in CFD, Examples for Resistance and Flow

1. PURPOSE OF PROCEDURE

Provide an example for the verification and validation methodology for a RANS CFD Code and results for steady flor for a cargo/container ship following the Quality Manual procedures 4.9-04-01-01, "Uncertainty Analysis in CFD, Uncertainty Assessment Methodology" and 4.9-04-01-02, "Uncertainty Analysis in CFD, Guidelines for RANS Codes."

2. EXAMPLE FOR RANS CFD CODE

Example results of verification and validation are presented for a single CFD code and for specified objectives, geometry, conditions, and available benchmark information. The CFD code is CFDSHIP-IOWA, which is a general-purpose, multi-block, high performance computing (parallel), unsteady RANS code (Paterson et al, 1998; Wilson et al., 1998) developed for computational ship hydrodynamics**.** The RANS equations are solved using higher-order upwind finite differences, PISO, k-w turbulence model, and exact and approximate treatments, respectively, of the kinematic and dynamic free-surface boundary conditions. The objectives are to demonstrate the usefulness of the proposed verification and validation procedures and methodology and establish the levels of verification and validation of the simulation results for an established benchmark for ship hydrodynamics CFD validation. The section references and

are to QM procedure 4.9-04-01-01 and the equation numbering is contiguous with QM procedure 4.9-04-01-01.

2.1 Geometry, Conditions, and Benchmark Data

The geometry is the Series 60 cargo/container ship. The Series 60 was used for two of the three test cases at the last international workshop on validation of ship hydrodynamics CFD codes (CFD Workshop Tokyo, 1994). The conditions for the calculations are Froude number $Fr = 0.316$, Reynolds number $Re = 4.3 \times 10^6$, and zero sinkage and trim. These are the same conditions as the experiments, except the resistance and sinkage and trim tests, as explained next. The variables selected for verification and validation are resistance C_T (integral variable) and wave profile ζ (point variable).

The benchmark data is provided by Toda et al. (1992), which was also the data used for the Series 60 test cases at the CFD Workshop Tokyo (1994). The data includes resistance and sinkage and trim for a range of Fr for the model free condition (i.e., free to sink and trim); and wave profiles, near-field wave pattern, and mean velocities and pressures at numerous stations from the bow to the stern and near wake, all for $Fr = (0.16, 0.316)$ and the zero sinkage and trim model fixed condition. The data also includes uncertainty estimates, which were recently

	ITTC - Quality Manual	4.9 – 04
ITTC 1999 22nd		02 – 01 Page 3 of 12
	CFD General **Uncertainty Analysis in CFD** **Examples for Resistance and Flow**	Effective Date | Revision 00

confirmed/updated by Longo and Stern (1999) closely following standard procedures (Coleman and Steele, 1999).

The resistance is known to be larger for free vs. fixed models. Data for the Series 60 indicates about an 8% increase in C_T for the free vs. fixed condition over a range of Fr including Fr=0.316 (Ogiwara and Kajatani, 1994). The Toda et al. (1992) resistance values were calibrated (i.e., reduced by 8%) for effects of sinkage and trim for the present comparisons.

2.2 Computational Grids

Grid studies were conducted using four grids (m=4), which enables two separate grid studies to be performed and compared. Grid study 1 gives estimates for grid errors and uncertainties on grid 1 using the three finest grids 1-3 while grid study 2 gives estimates for grid errors and uncertainties on grid 2 using the three coarsest grids 2-4. The results for grid study 1 are given in detail and the differences for grid study 2 are also mentioned. The grids were generated using the commercial code GRIDGEN (Pointwise, Inc.) with consideration to topology; number of points and grid refinement ratio r_G; near-wall spacing and k-w turbulence model requirement that first point should be at y^+<1; bow and stern spacing; and free-surface spacing.

The topology is body-fitted, H-type, and single block.. The sizes of grids 1 (finest) through 4 (coarsest) are 101x26x16 = 42,016, 144x36x22 = 114,048, 201x51x31 = 317,781, and 287x78x43 = 876,211 and the grid

refinement ratio $r_G = \sqrt{2}$. Clustering was used near the bow and stern in the x- direction, at the hull in the h-direction, and near the free surface in the z-direction. The y^+ values for grids 1-4 were about 0.7, 1, 1.4, and 2, respectively. About twice the number of grid points in the h-direction would be required to achieve $y^+ < 1.0$ for grids 1-4 (i.e., roughly 1,800,000 points on the finest grid). With grid refinement ratio $r_G = \sqrt{2}$, only grids 1 and 2 were generated. Grids 3 and 4 were obtained by removing every other point from grids 1 and 2, respectively (i.e., the grid spacing of grids 3 and 4 is twice that of grids 1 and 2, respectively). Grids 1 and 2 were generated by specifying the grid spacing at the corners and number of points along the edges of the computational blocks. The faces of the computational blocks were smoothed using an elliptic solver after which the coordinates in the interior were obtained using transfinite interpolation from the block faces. Grid 2 was generated from grid 1 by increasing the grid spacing and decreasing the number of computational cells in each coordinate direction at the corners of the blocks by a factor r_G. A comparison of the four grids at the free surface plane is shown in figure 1 along with computed wave elevation contours.

2.3 Verification and Validation of Integral Variable: Resistance

Verification. Verification was performed with consideration to iterative and grid convergence studies, i.e., $\delta_{SN} = \delta_I + \delta_G$ and $U_{SN}^2 = U_I^2 + U_G^2$.

	ITTC - Quality Manual	**4.9 – 04** **02 – 01**
ITTC 1999 22nd		Page 4 of 12
	CFD General **Uncertainty Analysis in CFD** **Examples for Resistance and Flow**	Effective Date | Revision 00

Iterative convergence was assessed by examining iterative history of ship forces and L2 norm of solution changes summed over all grid points. Figure 2 shows a portion of the iterative history on grid 1. The portion shown represents a computation started from a previous solution and does not reflect the total iterative history. Solution change drops four orders of magnitude from an initial value of about 10^{-2} (not shown) to a final value of 10^{-6}. The variation in C_T is about $0.2\%D$ over the last period of oscillation (i.e., $U_I = 0.2\%D$). Iterative uncertainty is estimated as half the range of the maximum and minimum values over the last two periods of oscillation (see figure 2c). Iterative histories for grids 2-4 show iterative uncertainties of about 0.02, 0.03, and 0.01%D, respectively. The level of iterative uncertainties for grids 2-4 are about two orders of magnitude less than the grid error and uncertainty. The iterative uncertainty for grid 1 is one order of magnitude smaller than the grid error. For all four grids the iteration errors and uncertainties are assumed to be negligible in comparison to the grid errors and uncertainties for all four solutions (i.e., $\delta_I << \delta_G$ and $U_I << U_G$ such that $\delta_{SN} = \delta_G$ and $U_{SN} = U_G$).

The results from the grid convergence study for C_T are summarized in tables 1 and 2. The solutions for C_T indicate the converging condition (i) of equation (16) with $R_G = \varepsilon_{21}/\varepsilon_{32} = 0.58$. The first-order RE estimate $\delta_{RE_{G_1}}$ [in equation (22)], order of accuracy p_G [in equation (23)], and correction factor C_G [in equation (24a)] are

$$\delta^*_{RE_{G_1}} = \left(\frac{\varepsilon_{21_G}}{r_G^{p_G}-1}\right) = \left(\frac{0.07x10^{-3}}{(\sqrt{2})^{1.6}-1}\right) \qquad (39)$$
$$= 0.09x10^{-3}$$

$$p_G = \frac{\ln(\varepsilon_{32_G}/\varepsilon_{21_G})}{\ln(r_G)} \qquad (40)$$
$$= \frac{\ln(0.12/0.07)}{\ln(\sqrt{2})} = 1.6$$

$$C_G = \frac{r_G^{p_G}-1}{r_G^{p_{G_{est}}}-1} = \frac{(\sqrt{2})^{1.6}-1}{(\sqrt{2})^2-1} = 0.74 \qquad (41)$$

where $p_{est} = p_{th} = 2$ was used in equation (41). Uncertainty and error estimates are made next both considering C_G as sufficiently less than or greater than 1 and lacking confidence and C_G as close to 1 and having confidence, as discussed in Section 3.2.3.

For $C_G = 0.74$ considered as sufficiently less than or greater than 1 and lacking confidence, U_G is estimated and not δ^*_G

$$U_G = \left|C_G\delta^*_{RE_{G_1}}\right| + \left|(1-C_G)\delta^*_{RE_{G_1}}\right| \qquad (42)$$
$$= 0.07x10^{-3} + 0.02x10^{-3} = 0.09x10^{-3}$$

U_G is 1.8% S_{G_1}.

For $C_G = 0.74$ considered close to 1 and having confidence, both and δ^*_G and U_{G_C} are estimated

$$\delta^*_{G_1} = C_G\delta^*_{RE_{G_1}} = 0.07x10^{-3} \qquad (43)$$

$$U_{G_C} = \left|(1-C_G)\delta^*_{RE_{G_1}}\right| = 0.02x10^{-3} \qquad (44)$$

The corrected solution S_C is defined with $S = S_{G_1}$

$$S_C = S_{G_1} - \delta^*_{G_1} = 4.96x10^{-3} \qquad (45)$$

$\delta^*_{G_1}$ and U_{G_C} are 1.4% and 0.4% S_C, respectively. In both cases, the level of verification is relatively small <2%.

Table 2 includes results for grid study 2, which are similar to those for gird study 1, but the values are larger by a factor of about 2, except S_C which differs by only 0.4%. Also shown in table 1 are C_P and C_F. C_F comprises about 70% of C_T and also displays convergence; however, C_P indicates oscillatory convergence. Relatively small C_G and oscillatory C_P suggests that the solutions are relatively far from the asymptotic range. Another reason for oscillatory C_P is that different flow phenomena may be resolved for the finer than the coarser grids.

Validation. Validation is performed using both the simulation prediction S and the corrected simulation prediction S_C, as summarized in table 3. First using S, the comparison error is calculated from equation (30) with $S = S_{G_1}$ as

$$E = D - S = 5.42x10^{-3} - 5.03x10^{-3}$$
$$= 0.39x10^{-3} = 7.2\%D \qquad (46)$$

The validation uncertainty is calculated from equation (33) as

$$U_V = \sqrt{U_{SN}^2 + U_D^2} = 0.17x10^{-3} = 3.1\%D \qquad (47)$$

where $U_{SN}=U_G =1.7\%D$ and $U_D=2.5\%D$. Comparison error $|E|>U_V$ such that the simulation results are not validated. U_{SN} and U_D are of similar order such that reduction in U_V would require reduction of U_D and U_{SN} (e.g., use of finer grids for U_{SN}). E is positive, i.e., the simulation under predicts the data. The trends shown in table 1 suggest C_p too small. Presumably modeling errors such as resolution of the wave field and inclusion of effects of sinkage and trim can be addressed to reduce E and validate C_T at $U_V=3.1\%$D; however, the case for this reasoning is stronger when considering the corrected comparison error, as discussed next.

Second using S_C, the corrected comparison error is calculated from equation (34) as

$$E_C = D - S_C = 5.42x10^{-3} - 4.96x10^{-3}$$
$$= 0.46x10^{-3} = 8.5\%D \qquad (48)$$

The validation uncertainty is calculated from equation (35) as

$$U_{V_c} = \sqrt{U_{S_cN}^2 + U_D^2} = 0.14x10^{-3} = 2.6\%D \qquad (49)$$

where $U_{S_cN} = U_{G_c} = 0.4\%D$. Here again, $|E_C| > U_{V_c}$ such that the simulation results are not validated. However, validation uncertainty U_{V_c} is relatively small and $U_{S_cN} << U_D$ more strongly suggests than was the case for E that E_C is mostly due to modeling errors. Therefore modeling issues should/can be improved to reduce E_C and validate C_T at the reduced level $U_{V_c} = 2.6\%D$ in comparison to equation (47).

The results from grid study 2 are summarized in table 4. The results are similar to those for grid study 1, but E and E_C are smaller and U_V and U_{V_c} are larger.

2.4 Verification and Validation of a Point Variable: Wave Profile

Verification. Verification for the wave profile was conducted as per that described for the resistance in Section 4.3 with the distinction that a point variable is defined over a distribution of grid points. Interpolation of the wave profile on all grids onto a common

distribution is required to compute solution changes. Since calculation of the comparison error $E=D-S$ is required for validation, wave profiles on grids 1-4 are interpolated onto the distribution of the data. The same four grids were used and, here again iteration errors and uncertainties were negligible in comparison to the grid errors and uncertainties for all four solutions, i.e., $\boldsymbol{d}_I << \boldsymbol{d}_G$ and $U_I << U_G$ such that $\boldsymbol{d}_{SN} = \boldsymbol{d}_G$ and $U_{SN} = U_G$.

R_G at local maximums and minimums (i.e., $x/L = 0.1$, 0.4, and 0.65 in figure 3a) and based on L2 norm solution changes both show convergence. The spatial order of accuracy for the wave profile was computed from the L2 norm of solution changes

$$\langle p_G \rangle = \frac{\ln\left(\left\|\boldsymbol{e}_{32_G}\right\|_2 / \left\|\boldsymbol{e}_{21_G}\right\|_2\right)}{\ln(r_G)} = 1.4 \qquad (50)$$

where $< >$ is used to denote a profile-averaged value and $\left\|\boldsymbol{e}\right\|_2$ denotes the L2 norm of solution change over the N points in the region, $0 < x/L < 1$

$$\left\|\boldsymbol{e}\right\|_2 = \left[\sum_{i=1}^{N} \boldsymbol{e}_i^2\right]^{1/2} \qquad (51)$$

Correction factor is computed from equation (24a) using order of accuracy p_G in equation (50) and $p_{G_{est}} = 2.0$

$$\langle C_G \rangle = \frac{r_G^{\langle p_G \rangle} - 1}{r_G^{p_{G_{est}}} - 1} = \frac{(\sqrt{2})^{1.4} - 1}{(\sqrt{2})^2 - 1} = 0.60 \qquad (52)$$

The estimates for order of accuracy and correction factor in equations (50) and (51) were used to estimate grid error and uncertainty for the wave profile at each grid point.
For $<C_G> = 0.60$ considered as sufficiently less than or greater than 1 and lacking confidence, pointwise values for U_G are

estimated and not $\boldsymbol{d}_G^*$. Equation (26) is used to estimate U_G

$$U_G = \left|\langle C_G \rangle \left(\frac{\boldsymbol{e}_{21_G}}{r_G^{\langle p_G \rangle} - 1}\right)\right|$$
$$+ \left|(1 - \langle C_G \rangle)\left(\frac{\boldsymbol{e}_{21_G}}{r_G^{\langle p_G \rangle} - 1}\right)\right| \qquad (53)$$

For $<C_G>=0.60$ considered close to 1 and having confidence, pointwise values for both $\boldsymbol{d}_G^*$ and U_{G_c} are estimated using equations (25) and (27)

$$\boldsymbol{d}_{G_1}^* = \langle C_G \rangle\left(\frac{\boldsymbol{e}_{21_G}}{r_G^{\langle p_G \rangle} - 1}\right) \qquad (54)$$

$$U_G = \left|(1 - \langle C_G \rangle)\left(\frac{\boldsymbol{e}_{21_G}}{r_G^{\langle p_G \rangle} - 1}\right)\right| \qquad (55)$$

Equation (10) is used to calculate S_C at each grid point
$$S_C = S_{G_1} - \boldsymbol{d}_{G_1}^* \qquad (56)$$
The results are summarized in table 5. The level of verification is similar to that for C_T with slightly higher values. Table 5 includes results for grid study 2, which are much closer to those for grid study 1 than was the case for C_T.

Validation. Validation of the wave profile is performed using both the simulation prediction S and the corrected simulation prediction S_C . Profile-averaged values for both definitions of the comparison error, validation uncertainty, and simulation uncertainty are given in table 6. Values are normalized with the maximum value for the wave profile $\boldsymbol{z}_{max}=0.014$ and the uncertainty in the data was reported to be $3.7\%\boldsymbol{z}_{max}$. E is nearly validated at about 5%. The trends are similar to those for C_T, except there are

smaller differences between the use of E and E_C.

The point comparison error $E=D$-S is compared to validation uncertainty U_V in figure 3b, while error $E_C=D$-S_C is compared to validation uncertainty U_V in figure 3d. In the latter case, the validation uncertainty U_V in figure 3d is mostly due to U_D. Much of the profile is validated. The largest errors are at the crests and trough regions, i.e., bow, shoulder, and stern waves.

The results from grid study 2 are summarized in table 7 and included in Figure 3. The results are similar to those for grid study 1, but both E and E_C and U_V and U_{V_C} are larger.

3. REFERENCES

CFD Workshop Tokyo 1994, 1994, Proceedings, Vol. 1 and 2, 1994, Ship Research Institute Ministry of Transport Ship & Ocean Foundation.

Longo, J. and Stern, F., "Resistance, Sinkage and Trim, Wave Profile, and Nominal Wake and Uncertainty Assessment for DTMB Model 5512," Proc. 25th ATTC, Iowa City, IA, 24-25 September 1998.

Ogiwara, S. and Kajitani, H., 1994, "Pressure Distribution on the Hull Surface of Series 60 (C_B=0.60) Model," Proceedings CFD Workshop Tokyo, Vol. 1, pp. 350-358.

Paterson, E.G., Wilson, R.V., and Stern, F., 1998, "CFDSHIP-IOWA and Steady Flow RANS Simulation of DTMB Model 5415," 1st Symposium on Marine Applications of Computational Fluid Dynamics, McLean, VA, 19-21 May.

Toda, Y., Stern, F., and Longo, J., 1992, "Mean-Flow Measurements in the Boundary Layer and Wake and Wave Field of a Series 60 C_B = .6 Model Ship - Part 1: Froude Numbers .16 and .316," Journal of Ship Research, Vol. 36, No. 4, pp. 360-377.

Wilson, R., Paterson, E., and Stern, F., 1998 "Unsteady RANS CFD Method for Naval Combatant in Waves," Proc. 22nd ONR Symposium on Naval Hydro, Washington, DC.

Table 1 Grid convergence study for total C_T, pressure C_P, and frictional C_F resistance ($x10^{-3}$) for Series 60.

Grid	Grid 4 101x26x16	Grid 3 144x36x22	Grid 2 201x51x31	Grid 1 287x71x43	Data
C_T **e**	5.72	5.22 -8.7%	5.10 -2.3%	5.03 -1.3%	5.42
C_P **e**	1.95	1.63 -16.4%	1.64 +0.6%	1.61 -1.8%	$C_R = 2.00$
C_F **e**	3.78	3.59 -5.0%	3.46 -3.6%	3.42 -1.2%	3.42 ITTC

% of finer grid value.

Table 2. Verification of total resistance C_T ($x10^{-3}$) for Series 60.

Study	R_G	p_G	C_G	U_G	d_G^*	U_{G_C}	S_C
1 *(grids 1-3)*	0.57	1.6	0.74	1.8%	1.4%	0.4%	4.96
2 *(grids 2-4)*	0.24	4.1	3.1	3.9%	2.4%	1.6%	4.98

%S_G.

Table 3. Validation of total resistance for Series 60 – study 1 (grids 1-3).

	E%	$U_V\%$	$U_D\%$	$U_{SN}\%$
$E=D-S$	7.2	3.1	2.5	1.7
$E_C=D-S_C$	8.5	2.6	2.5	0.4

%D.

Table 4. Validation of total resistance for Series 60 – study 2 (grids 2-4).

	E%	$U_V\%$	$U_D\%$	$U_{SN}\%$
$E=D-S$	5.9	4.4	2.5	3.7
$E_C=D-S_C$	8.1	3.0	2.5	1.5

%D.

Table 5 Profile-averaged values from verification of wave profile for Series 60.

Study	R_G	p_G	C_G	U_G	U_{G_C}
1 (grids 1-3)	0.62	1.4	0.60	2.6%	1.0%
2 (grids 2-4)	0.64	1.3	0.57	3.6%	1.4%

$\%\zeta_{max}$.

Table 6. Profile-averaged values from validation
of wave profile for Series 60 – study 1 (grids 1-3).

	E%	$U_V\%$	$U_D\%$	$U_{SN}\%$
$E=D-S$	5.2	4.5	3.7	2.6
$E_C=D-S_C$	5.5	3.8	3.7	1.0

$\%\zeta_{max}$.

Table 7. Profile-averaged values from validation
of wave profile for Series 60 – study 2 (grids 2-4).

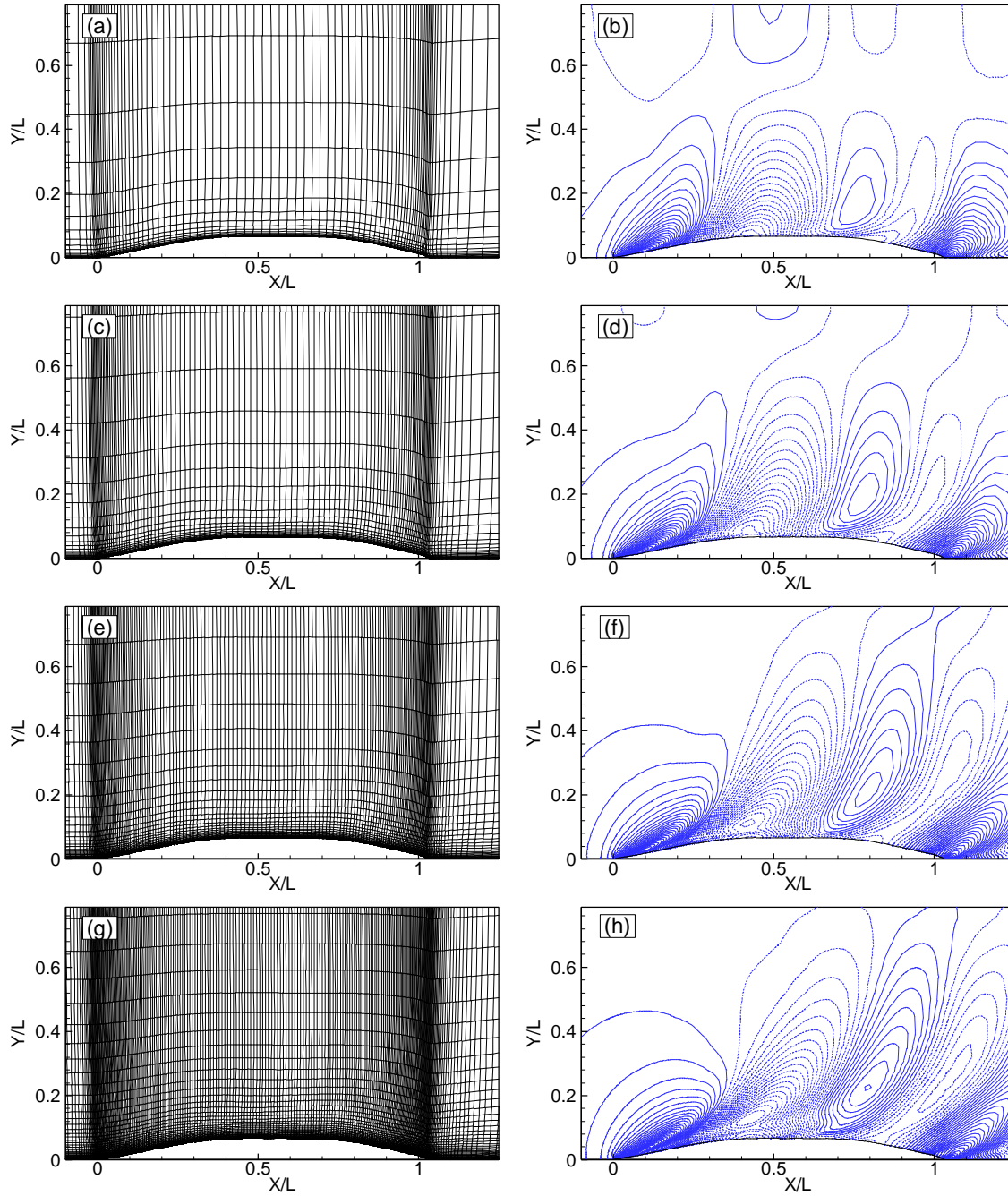|	E%	$U_V\%$	$U_D\%$	$U_{SN}\%$
$E=D-S$	5.5	5.1	3.7	3.6
$E_C=D-S_C$	6.6	3.9	3.7	1.4

$\%\zeta_{max}$.

Figure 1. Grids and wave contours from verification and validation studies for Series 60: (a) and (b) coarsest - grid 4; (c) and (d) grid 3; (e) and (f) grid 2; and (g) and (h) finest - grid 1.
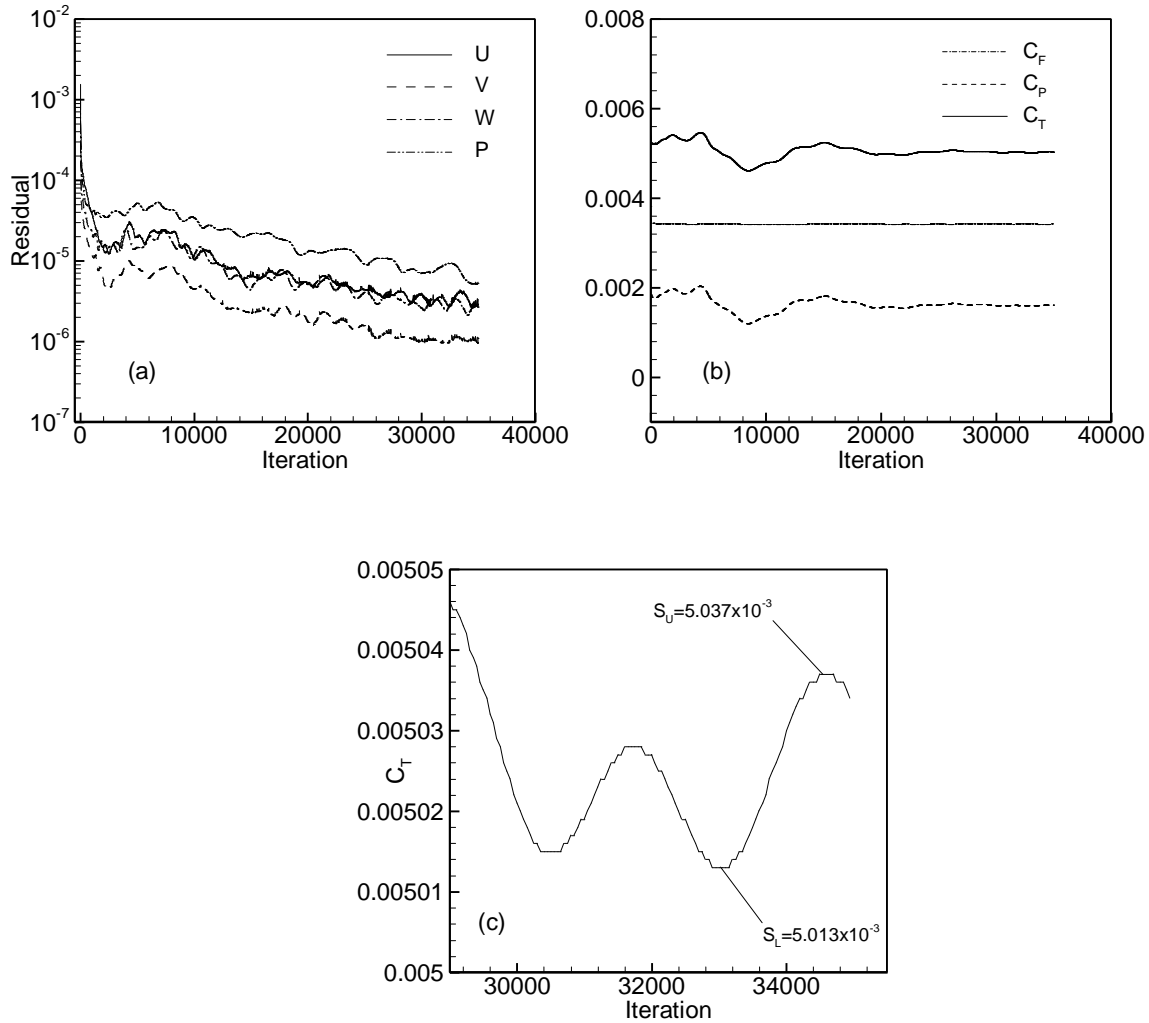
Figure 2. Iteration history for Series 60 on grid 1: (a) solution change, (b) ship forces - C_F, C_P, and C_T and (c) magnified view of total resistance C_T over last two periods of oscillation.
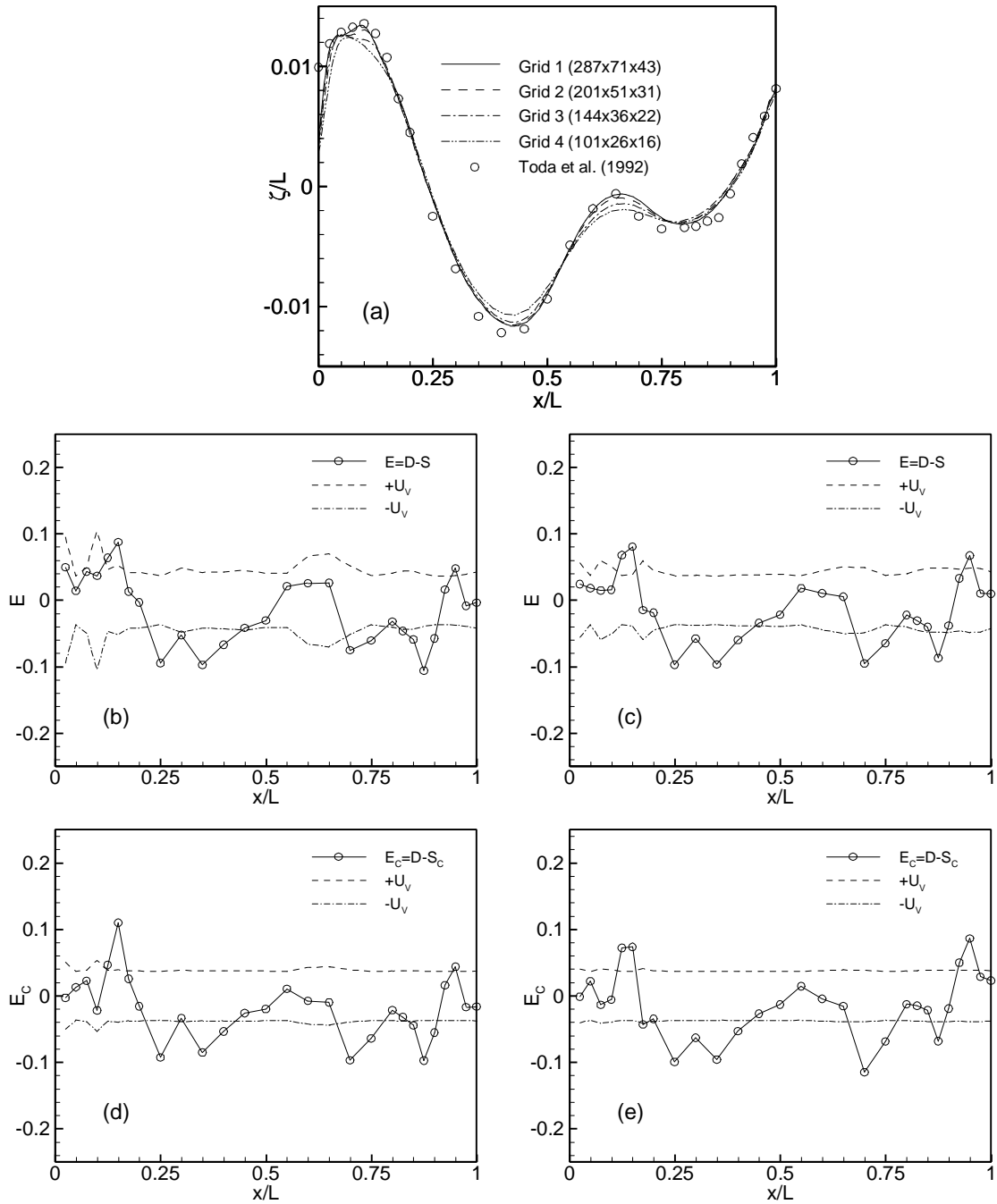
Figure 3. Wave profile for Series 60: (a) grid study; (b) and (d) validation using grids 2-4; and (c) and (e) validation using grids 1-3.